JBC ARTICLE

# The anion transporter SLC26A9 localizes to tight junctions and is degraded by the proteasome when co-expressed with F508del–CFTR

Received for publication, July 12, 2019, and in revised form, October 21, 2019 Published, Papers in Press, October 23, 2019, DOI 10.1074/jbc.RA119.010192

**Yukiko Sato**[‡§1], **David Y. Thomas**[§¶], **and John W. Hanrahan**[‡§2]

*From the* [‡]*Department of Physiology, McGill University, Montréal, Québec H3G 1Y6, the* [¶]*Department of Biochemistry, McGill University, Montréal, Québec H3A 1A3, and the* [§]*Cystic Fibrosis Translational Research Center, McGill University, Montréal, Québec H3G 1Y6, Canada*

Edited by Roger J. Colbran

**Mutations in the gene encoding the cystic fibrosis transmembrane conductance regulator (CFTR) disrupt epithelial secretion and cause cystic fibrosis (CF). Available CFTR modulators provide only modest clinical benefits, so alternative therapeutic targets are being explored. The anion-conducting transporter solute carrier family 26 member 9 (SLC26A9) is a promising candidate, but its functional expression is drastically reduced in cells that express the most common CF-associated CFTR variant, F508del–CFTR, through mechanisms that remain incompletely understood. Here, we examined the metabolic stability and location of SLC26A9 and its relationship to CFTR. Compared with SLC26A9 levels in BHK cells expressing SLC26A9 alone or with WT–CFTR, co-expression of SLC26A9 with F508del–CFTR reduced total and plasma membrane levels of SLC26A9. Proteasome inhibitors increased SLC26A9 immunofluorescence in primary human bronchial epithelial cells (pHBEs) homozygous for F508del–CFTR but not in non-CF pHBEs, suggesting that F508del–CFTR enhances proteasomal SLC26A9 degradation. Apical SLC26A9 expression increased when F508del–CFTR trafficking was partially corrected by low temperature or with the CFTR modulator VX-809. The immature glycoforms of SLC26A9 and CFTR co-immunoprecipitated, consistent with their interaction in the endoplasmic reticulum (ER). Transfection with increasing amounts of WT–CFTR cDNA progressively increased SLC26A9 levels in F508del–CFTR-expressing cells, suggesting that WT–CFTR competes with F508del–CFTR for SLC26A9 binding. Immunofluorescence staining of endogenous SLC26A9 and transfection of a 3HA-tagged construct into well-differentiated cells revealed that SLC26A9 is mostly present at tight junctions. We conclude that SLC26A9 interacts with CFTR in both the ER and Golgi and that its interaction with F508del–CFTR increases proteasomal SLC26A9 degradation.**

The airway surface liquid (ASL)[3] is a thin layer of fluid that lines the conducting airways and plays a crucial role in the mucociliary clearance of inhaled pathogens (1). The volume and composition of the ASL determine the efficiency of mucociliary clearance and are tightly regulated by epithelial ion and fluid secretion (1, 2). An important channel mediating airway anion secretion is the cystic fibrosis transmembrane conductance regulator (CFTR) (3–5), a cAMP/protein kinase A–regulated channel in the ABC transporter family that has two membrane-spanning domains (MSD1 and MSD2), two nucleotide-binding domains (NBD1 and NBD2), and a regulatory (R) domain (3, 6–8). Loss– of–function mutations in CFTR impair anion and fluid secretion and increase the susceptibility of airways to infection (9, 10).

The most common CFTR mutation is a deletion of phenylalanine at position 508 (F508del–CFTR), which causes misfolding and retention of the mutant in the endoplasmic reticulum (ER) and its rapid degradation by the ubiquitin–proteasome pathway (11, 12). CFTR correctors (*i.e.* small molecule pharmacological chaperones that partially restore the folding and trafficking of this mutant) have been described; however, they provide modest clinical benefit and only for a subset of patients (13). Thus, there is increasing interest in alternative anion efflux pathways as potential therapeutic targets, such as the $Cl^-$ conductance SLC26A9 (14–19). SLC26A9 activity protects mice from mucus airway obstruction, and polymorphisms in

This work was supported by Grant 608466 from Cystic Fibrosis Canada (to J. W. H.) and Grant PJT-156183 from the Canadian Institutes of Health Research (CIHR) (to J. W. H. and D. Y. T.). The authors declare that they have no conflicts of interest with the contents of this article.

This article contains Fig. S1.

[1] Recipient of scholarships from Cystic Fibrosis Canada, Fonds de la Recherche en Santé du Québec (FQRS), Canadian Institutes of Health Research, and the Groupe de Recherche Axé sur la Structure des Protéines.

[2] To whom correspondence should be addressed: Dept. of Physiology, Cystic Fibrosis Translational Research Centre, McGill University, 3655 Promenade Sir William Osler, Montréal, Québec H3G 1Y6, Canada. Tel.: 514-398-8320; E-mail: john.hanrahan@mcgill.ca.

[3] The abbreviations used are: ASL, airway surface liquid; CFTR, cystic fibrosis transmembrane conductance regulator; SLC26A9, solute carrier family 26 member 9; pHBE, primary bronchial epithelial; CF, cystic fibrosis; MSD, membrane-spanning domain; NBD, nucleotide-binding domain; R domain, regulatory domain; STAS, sulfate transporter and anti-$\sigma$ factor antagonist; CAL, CFTR-associated ligand; DAPI, 4′,6-diamidino-2-phenylindole; ER, endoplasmic reticulum; FMP, FLIPR membrane potential; BHK, baby hamster kidney; CQ, chloroquine; qPCR, quantitative polymerase chain reaction; HEK293, human embryonic kidney 293 cells; CFBE41o−, human cystic fibrosis bronchial epithelial cell line; HA, human influenza hemagglutinin; MUC5AC, Mucin 5AC; ZO-1, zonula occludens-1, NHERF1, sodium–hydrogen antiporter 3 regulator 1; ANOVA, analysis of variance; GAPDH, glyceraldehyde-3-phosphate dehydrogenase; eGFP, enhanced GFP; PFA, paraformaldehyde; ALI, air–liquid interface; HBE cell, human bronchial epithelial cell.

the SLC26A9 gene that reduce its expression in human airways are associated with asthma (20). Genome-wide association studies have also identified SLC26A9 as a modifier of CF severity and CFTR potentiator efficacy, and several groups have reported interactions between SLC26A9 and CFTR (21–24).

SLC26A9 has a transmembrane domain with putative *N*-glycosylation sites at asparagine 153 and asparagine 156, a STAS (sulfate transporter and anti-$\sigma$ factor antagonist) domain, and a C-terminal PDZ domain-binding motif (25). SLC26A9 can be co-immunoprecipitated with both WT–CFTR and F508del–CFTR using lysates of human embryonic kidney 293 (HEK293) cells or the human cystic fibrosis bronchial epithelial cell line CFBE41o− (14, 17). Interaction between the STAS domain of SLC26A9 and the R domain of CFTR has been shown biochemically using purified recombinant domains (16), and interaction between the STAS domain of a closely-related protein (SLC26A3) and the R domain of CFTR was demonstrated using NMR (26). Importantly, Bertrand *et al.* (14) found that SLC26A9-dependent currents can be measured when SLC26A9 is co-expressed with WT–CFTR in HEK293 cells, but not when co-expressed with F508del–CFTR. Although whole-cell SLC26A9 levels, including the mature glycoform, were similar when SLC26A9 was overexpressed with WT or mutant CFTR in HEK cells, plasma membrane expression of SLC26A9 was reduced in the presence of F508del–CFTR, and it was co-immunoprecipitated with the Golgi-localized PDZ protein CAL (CFTR-associated ligand (27)). Recently, CAL has also been demonstrated in the ER (28); however, potential degradation of SLC26A9 by the proteasomal pathway at the ER has not been investigated.

It is important to understand the SLC26A9 trafficking abnormality induced by F508del–CFTR as it is a hurdle for the development of SLC26A9 as a therapeutic target. Approximately 90% of individuals with CF have at least one F508del–CFTR allele. Here, we confirm that SLC26A9 surface expression is diminished by F508del–CFTR and then examine the mechanism of premature degradation using inhibitors, surface biotinylation, fluorescence microscopy, and functional assays. In addition to CAL-dependent degradation at the Golgi, as described previously (27), the present results reveal a novel mechanism in which F508del–CFTR causes the retention of SLC26A9 at the ER and degradation by the proteasome. Although interaction with WT–CFTR was observed and may normally enhance the maturation and trafficking of SLC26A9 in well-differentiated primary human bronchial epithelial (pHBE) cells, the latter was localized at tight junctions and had much faster turnover at the cell surface compared with CFTR. These findings clarify the dependence of SLC26A9 on CFTR and support the development of disruptors of the SLC26A9–F508del–CFTR interaction as a therapeutic strategy for CF.

## Results

### *F508del reduces SLC26A9 expression*

To examine the influence of CFTR on SLC26A9 protein expression and trafficking, we transfected 3HA–SLC26A9 into parental baby hamster kidney (BHK) cells lacking CFTR (BHK–parental) and also into BHK cell lines that stably express WT–CFTR (BHK–WT) or F508del–CFTR (BHK–F508del) and then immunoblotted 48 h later for SLC26A9. SLC26A9 expression was consistently much lower in BHK–F508del cells than in BHK–WT cells and was about half that in BHK–parental cells devoid of CFTR (Fig. 1, *A* and *B*). These results indicate that F508del–CFTR has a negative effect on steady-state SLC26A9 expression and is more deleterious than the complete absence of CFTR, evidence that SLC26A9 may be retained intracellularly and degraded prematurely as described for F508del–CFTR. The immunoblots revealed two SLC26A9 bands that likely represent the immature, nonglycosylated form (band B) and the mature, complex-glycosylated form (band C), as shown for CFTR (29). The immature band B glycoform of SLC26A9 was diminished in F508del–CFTR-expressing cells while band C SLC26A9 was still present, suggesting that some SLC26A9 maturation still occurs despite F508del–CFTR. For comparison, we examined SLC26A9 levels in a BHK cell line that stably expresses G551D–CFTR, a mutant with defective channel gating that traffics normally to the plasma membrane. When co-expressed with G551D–CFTR, SLC26A9 levels were intermediate between those with BHK–WT and BHK–F508del and slightly higher than in parental cells that lack CFTR completely (Fig. 1*B*). This further suggests that SLC26A9 may be degraded prematurely along with F508del–CFTR. SLC26A9 mRNA levels were similar in all three cell lines as measured using quantitative PCR (qPCR) (Fig. 1*C*); therefore, the reduction in SLC26A9 expression by F508del–CFTR is not due to decreases in transfection efficiency or transcription.

To determine whether SLC26A9 trafficking to the plasma membrane in BHK cells is adversely affected by F508del–CFTR, cell-surface biotinylation assays were performed. As with whole-cell lysate protein levels, SLC26A9 expression at the plasma membrane was lower in BHK–F508del cells compared with BHK–WT cells (Fig. 1*D*). The function of SLC26A9 was also assessed in these cells using the FLIPR membrane potential (FMP) assay, which reports depolarization of the membrane potential due to $Cl^-$ efflux. A reduction in the SLC26A9-dependent change in membrane potential during challenge with low-$Cl^-$ solution was evident in cells co-expressing F508del–CFTR (Fig. 1*E*).

To examine whether F508del–CFTR also suppresses SLC26A9 in airway epithelial cells, pHBEs from non-CF and F508del homozygote donors were studied. We first confirmed the specificity of the antibody by transfecting 3HA–SLC26A9 into BHK cells and co-immunostaining with anti-SLC26A9 and anti-HA antibody (Fig. 1*F*). Nearly perfect co-localization was observed (Fig. 1*F*, *Merge*), and no signal was detected in neighboring cells that had not been transfected (Fig. 1*F*, brightfield). Specificity was further confirmed in pHBEs by transducing them with adenoviral eGFP–SLC26A9 and comparing eGFP fluorescence and immunofluorescence signals (Fig. 1*G*). Immunostaining was superimposable with the eGFP fluorescence and again was detected only in pHBE cells that had been successfully transduced by the eGFP–SLC26A9 adenovirus. Despite similar levels of SLC26A9 mRNA (Fig. 1*H*), immunofluorescence staining of SLC26A9 was clearly reduced in F508del/F508del pHBE cells compared with non-CF cells (Fig. 1, *I* and *J*), and similar results were obtained using a different anti-SLC26A9 antibody (data not shown). These results confirm

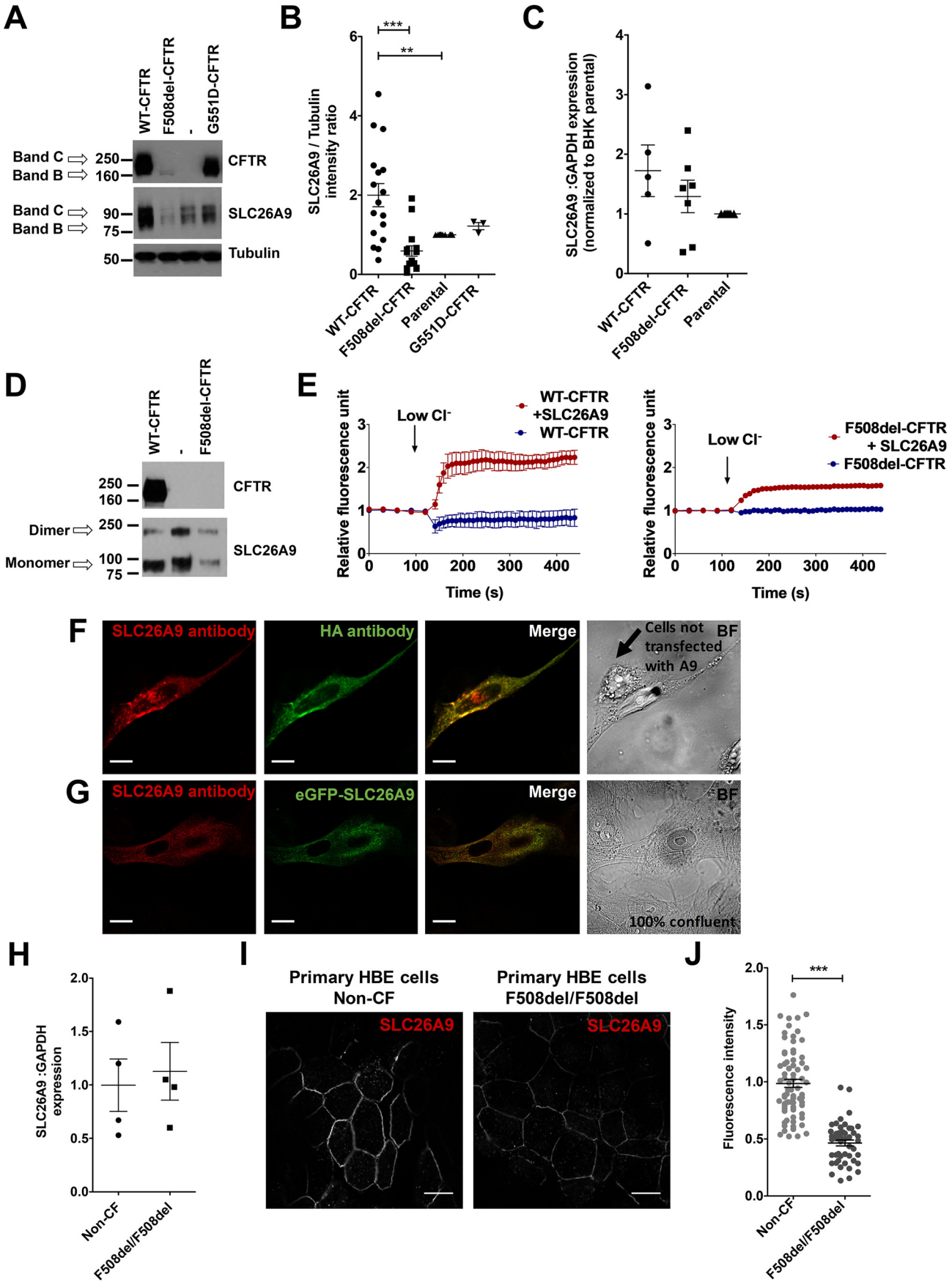
A
WT-CFTR
F508del-CFTR
-
G551D-CFTR
Band C
Band B
250
160
CFTR
90
75
SLC26A9
50
Tubulin
B
SLC26A9 / Tubulin intensity ratio
***
**
WT-CFTR
F508del-CFTR
Parental
G551D-CFTR
C
SLC26A9 :GAPDH expression (normalized to BHK parental)
WT-CFTR
F508del-CFTR
Parental
D
WT-CFTR
-
F508del-CFTR
CFTR
Dimer
Monomer
SLC26A9
E
Relative fluorescence unit
Low Cl-
WT-CFTR +SLC26A9
WT-CFTR
Time (s)
F508del-CFTR + SLC26A9
F508del-CFTR
F
SLC26A9 antibody
HA antibody
Merge
Cells not transfected with A9
BF
G
SLC26A9 antibody
eGFP-SLC26A9
Merge
BF
100% confluent
H
SLC26A9 :GAPDH expression
Non-CF
F508del/F508del
I
Primary HBE cells Non-CF
Primary HBE cells F508del/F508del
SLC26A9
SLC26A9
J
Fluorescence intensity
***
Non-CF
F508del/F508del

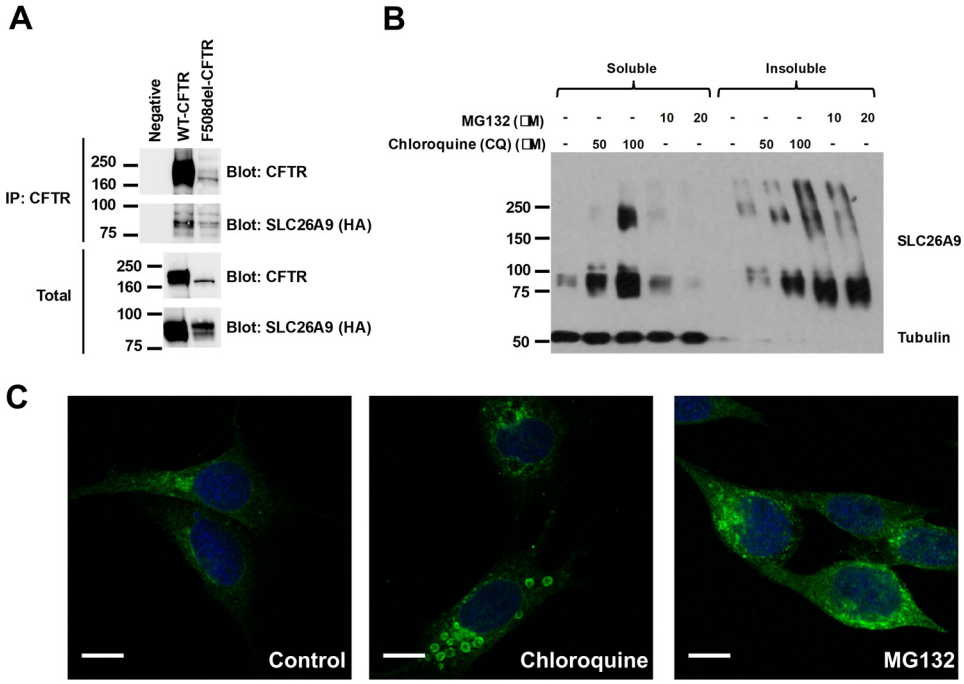


**Figure 2. SLC26A9 is degraded by both lysosomal and proteasomal pathways.** *A,* BHK–WT and BHK–F508del were transfected with SLC26A9, immunoprecipitated with CFTR antibody (M3A7), and immunoblotted for CFTR or SLC26A9. Figure is representative of three blots. *B,* BHK parental cells were transfected with 3HA–SLC26A9 cDNA and exposed 32 h later to MG132 or CQ at the concentrations indicated. After 16 h of treatment, cells were lysed, proteins were resolved by SDS-PAGE, and expression was detected by immunoblotting. Blot is representative of three experiments. *C,* BHK cells stably expressing SLC26A9 were treated with MG132 or CQ, fixed, and stained with mouse anti-HA antibody followed by goat anti-mouse Alexa-488. *Scale bar*, 10 $\mu$m. Images are representative of 18–40 total cells from three independent experiments.

that co-expression of F508del–CFTR reduces total and plasma membrane SLC26A9 expression when SLC26A9 is transfected into BHK cells or endogenously expressed at physiological levels in pHBE cells.

### *SLC26A9 is degraded by both proteasomal and lysosomal pathways*

Impaired folding of F508del–CFTR leads to its retention in the ER and premature degradation by the 26S proteasome (12). Because levels of band B SLC26A9 were reduced in BHK–F508del cells, we examined whether SLC26A9 interacts with F508del–CFTR by precipitating the latter using M3A7 antibody and probing the blots for SLC26A9. F508del–CFTR seemed to interact predominantly with band B SLC26A9, suggesting an association during biosynthesis (Fig. 2*A*). We then explored whether SLC26A9 is degraded by the proteasome pathway when F508del–CFTR is not present. SLC26A9 was transiently expressed in BHK–parental cells, which were then treated with the proteasome inhibitor MG132 or the lysosome inhibitor chloroquine (CQ). SLC26A9 expression was increased by CQ, suggesting it is at least partially degraded by the lysosome (Fig. 2*B*). Although there was no increase in soluble SLC26A9 in the lysate after treatment with MG132, there was a marked increase in the insoluble fraction due to polyubiquitination and aggregation (Fig. 2*B*). These results suggest that SLC26A9 undergoes degradation by both lysosomal and proteasomal pathways in the absence of CFTR. This was further indicated by an increase in overall SLC26A9 immunofluorescence upon treatment with either MG132 or CQ (Fig. 2*C*).

Pharmacological inhibitors were used to assess the role of CFTR in SLC26A9 degradation in BHK–WT and BHK–F508del cells. SLC26A9 fluorescence intensity and band intensity were increased in both cell lines after treatment with MG132 indicating proteasomal degradation, although it was difficult to determine whether there was more MG132-sensitive degradation in F508del–BHK cells, proba-

**Figure 1. SLC26A9 expression decreases when co-expressed with F508del–CFTR, compared with when it is expressed alone or with WT–CFTR.** *A,* BHK–WT, BHK–F508del, BHK parental, or BHK–G551D cells were transiently transfected with 3HA–SLC26A9. After 48 h, cells were lysed, and protein was resolved using SDS-PAGE, and expression was assessed by immunoblotting. Figure is representative of 3–18 experiments. *B,* SLC26A9 protein expression quantified by densitometry using ImageJ and normalized to tubulin in each sample. One-way ANOVA and Tukey's multiple comparison test were used. **, $p = 0.0013$; ***, $p = 0.0002$; $F = 10.6$ mean ± S.E., $n = 10$. *C,* SLC26A9 gene expression in transiently-transfected BHK cells was assessed using qPCR and quantified using $\Delta CT$ analysis, normalized to GAPDH expression, $n = 6$. *D,* membrane proteins labeled using sulfo-NHS-SS-biotin (0.5 $\mu$g/ml) and pulled down on streptavidin beads. Labeled proteins were resolved by SDS-PAGE, and expression was determined by immunoblotting. Blot shown is representative of $n = 4$ experiments. *E,* representative membrane potential measurements using the FMP assay in transiently-transfected BHK cells exposed to low-$Cl^-$ solution (see "Experimental procedures"). *F,* BHK cells were transiently transfected with 3HA–SLC26A9 and stained with anti-SLC26A9 and anti-HA to verify the specificity of the antibody. *G,* primary HBE cells were transduced with eGFP–SLC26A9 and immunostained using anti-SLC26A9 for comparison with the eGFP signal. *H,* SLC26A9 gene expression in well-differentiated pHBE cells from non-CF or F508del/F508del donors was determined using qPCR. Data represent the expression of SLC26A9 normalized to GAPDH ($n = 4$ for each). *I,* well-differentiated pHBE cells were isolated from healthy or F508del/F508del donors, scraped, cytospun, and fixed on coverslips. SLC26A9 was stained using rabbit anti-SLC26A9 antibody, and confocal images were taken at the apical pole. *J,* intensity of SLC26A9 immunofluorescence calculated from 45 to 70 cells in at least four independent experiments using ImageJ software. Student's *t* test; ***, $p < 0.001$ ($p = 2.7 \times 10^{-19}$) All *scale bars* are 10 $\mu$m.

bly due to the overexpression of both proteins (Fig. 3, *A–D*). However, when similar experiments were performed using well-differentiated non-CF and CF pHBE cells that express both proteins endogenously at their normal levels, MG132 treatment caused a more dramatic increase in SLC26A9 immunofluorescence in F508del/F508del cells (Fig. 3, *E* and *F*). These data suggest that SLC26A9 degradation by the proteasome is enhanced in cells that also express F508del–CFTR, depends on the stoichiometry of the two proteins, and is most evident when SLC26A9 and F508del–CFTR are expressed at physiological levels.

### *Correcting F508del–CFTR increases SLC26A9 expression*

To study the dependence of SLC26A9 on F508del–CFTR trafficking, we tested whether pharmacological rescue of the mutant CFTR could restore SLC26A9 expression. BHK–F508del cells were treated with the small molecule corrector VX-809, which was developed to improve the trafficking of F508del–CFTR, or incubated at 27 °C. VX-809 increased expression of mature (band C) F508del–CFTR, and this was accompanied by an increase in SLC26A9 protein (Fig. 4*A*). Similarly, when cells were incubated at low temperature, the amount of F508del–CFTR band C increased as did total SLC26A9 (Fig. 4*A*). Low temperature also enhanced the expression of both proteins at the cell surface (Fig. 4*B*). To test whether increased expression could be due to a direct effect of VX-809 or low temperature on SLC26A9 itself rather than F508del–CFTR, cells expressing only SLC26A9 were exposed to the corrector or 27 °C. VX-809 treatments had no effect on SLC26A9, and 27 °C caused only a slight increase that probably reflects modest improvement in folding efficiency at low temperature (Fig. 4*C*).

We noticed some mature SLC26A9 in the presence of F508del–CFTR suggesting it reaches the Golgi, whereas immature SLC26A9 was greatly reduced by F508del–CFTR compared with when SLC26A9 was expressed alone or with WT–CFTR. Together, these observations imply there are two populations of SLC26A9, one that is retained with F508del–CFTR and undergoes proteasomal degradation at the ER, and another noninteracting population that traffics to the plasma membrane. To test this hypothesis, clonal BHK cell lines stably co-expressing F508del–CFTR together with varying amounts of SLC26A9 were prepared. We selected one clone with low SLC26A9 expression (clone 5) and another clone with relatively high expression (clone 6) for further study (Fig. 4*D*). SLC26A9 levels were elevated slightly in both clone 5 (Fig. 4*D*, *exposure 1*) and clone 6 (Fig. 4*D*, exposure 2) after exposure to VX-809 or 27 °C. FMP assays confirmed that constitutive $Cl^-$ conductance was higher in clone 6 than clone 5, consistent with higher SLC26A9 protein expression. However, the additional SLC26A9 conductance induced by partial rescue of F508del–CFTR using VX-809 was not significant (Fig. 4*E*).

We then examined the effect of VX-809 on SLC26A9 levels in well-differentiated pHBE cells for comparison with BHK clones 5 and 6. SLC26A9 immunofluorescence increased when F508del/F508del pHBEs were treated with VX-809, consistent with elevated expression at the plasma membrane (Fig. 4, *F* and *G*). Together, these results suggest that rescuing F508del–CFTR reduces ER retention and proteasomal degradation of SLC26A9, although the impact depends on SLC26A9/CFTR stoichiometry and is less noticeable when SLC26A9 is overexpressed.

### *Expressing WT–CFTR rescues SLC26A9 from down-regulation by F508del–CFTR*

If WT–CFTR and F508del–CFTR interact with SLC26A9 at the same site, they might bind competitively. To test this, we transiently co-transfected BHK–F508del cells with SLC26A9 cDNA + increasing amounts of WT–CFTR cDNA (Fig. 5*A*). Immunoblots revealed that SLC26A9 expression increased progressively as the amount of CFTR cDNA (and hence CFTR protein expression) was increased, with maximal SLC26A9 levels observed using 0.2 $\mu$g of WT–CFTR plasmid. Forskolin-stimulated, Cl-dependent membrane potential responses were proportional to the amount of WT–CFTR cDNA used, indicating successful transfection with WT–CFTR (Fig. 5*B*). SLC26A9 function (measured in the absence of forskolin) was also progressively increased as measured using the FMP assay (Fig. 5*C*). Although a clear increase in band C CFTR was not detected, this was likely due to the low level of CFTR expression and limited sensitivity of immunoblots. These results show that WT–CFTR can relieve the inhibition of SLC26A9 expression by F508del–CFTR suggestive of competitive binding to SLC26A9, although this remains to be confirmed using biochemical methods.

### *Degradation of immature SLC26A9 is CFTR-dependent*

We next compared the rate of SLC26A9 degradation when it is expressed alone or together with WT- or F508del–CFTR. BHK cells were transfected with SLC26A9 and treated with the protein synthesis inhibitor cycloheximide for 0–6 h and then metabolic stability of SLC26A9 and CFTR was assessed by immunoblotting at multiple time points. CFTR band B declined in WT- and F508del–CFTR cells consistent with partial processing to the mature form and degradation by the proteasome (Fig. 6, *A* and *B*). Band C CFTR was observed in BHK–WT cells after inhibiting translation for 6 h, consistent with stable surface expression and/or efficient recycling of WT–CFTR at the plasma membrane (Fig. 6, *A* and *C*). Interestingly, the degradation of immature SLC26A9 was faster in cells expressing F508del than in cells expressing WT–CFTR or those lacking CFTR completely (compare band B degradation rates in Fig. 6*B*), yet the degradation of mature SLC26A9 occurred at a similar rate in all three cell lines. These results suggest that only immature SLC26A9 has reduced metabolic stability in the presence of F508del–CFTR, consistent with its premature degradation in the ER together with immature F508del–CFTR. They also raise the question as to why SLC26A9 and CFTR degradation rates are so different.

### *SLC26A9 is endocytosed more rapidly than CFTR*

SLC26A9 was eliminated within 4 h following treatment with cycloheximide, whereas band C CFTR remained nearly constant for at least 6 h and was still significant after 24 h (data not shown). Although CFTR is efficiently recycled from endosomes to the plasma membrane, little is known regarding SLC26A9

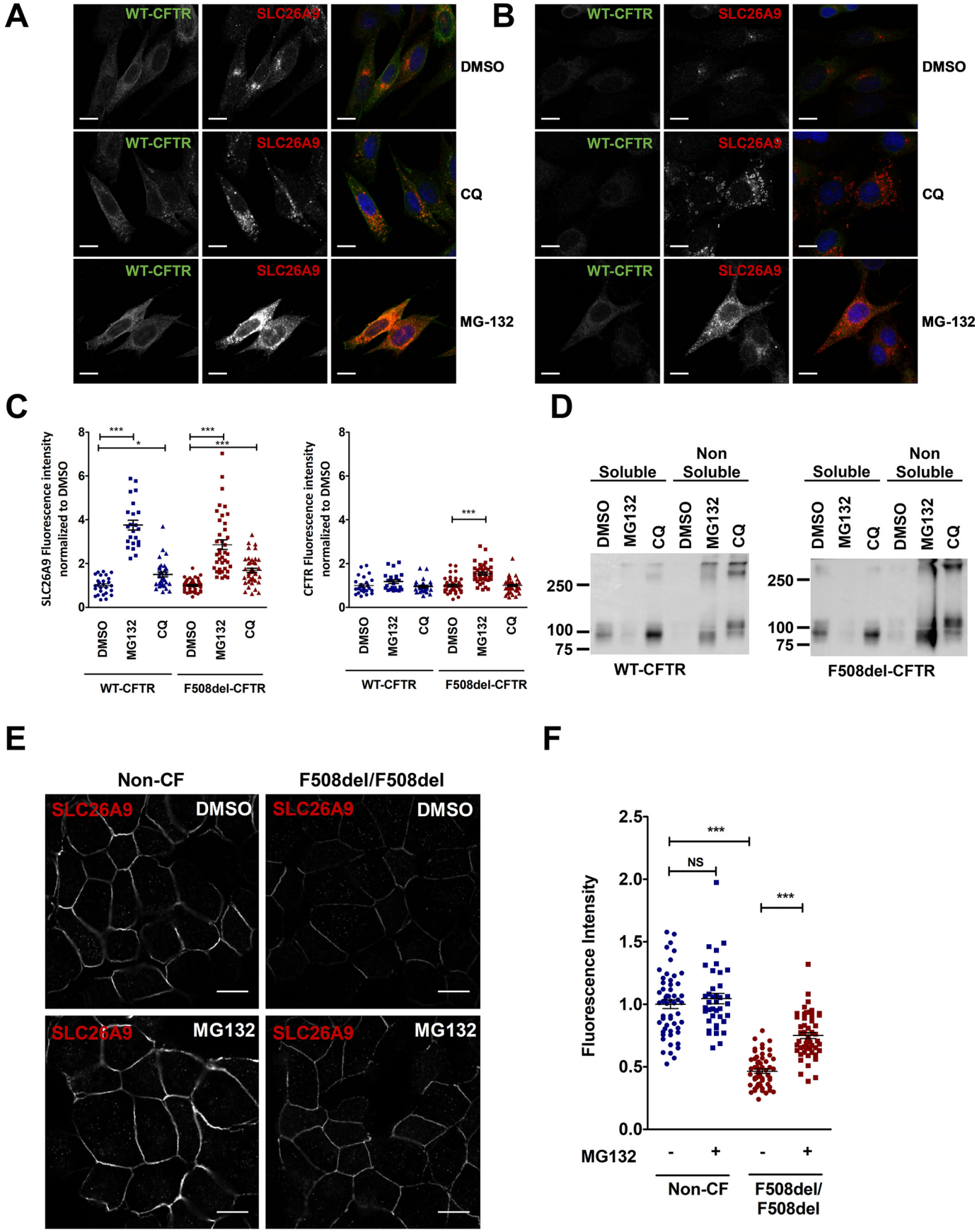
A
WT-CFTR
SLC26A9
DMSO
CQ
MG-132
B
C
SLC26A9 Fluorescence intensity normalized to DMSO
CFTR Fluorescence intensity normalized to DMSO
DMSO
MG132
CQ
WT-CFTR
F508del-CFTR
D
Soluble
Non Soluble
250
100
75
E
Non-CF
F508del/F508del
SLC26A9
DMSO
MG132
F
Fluorescence Intensity
NS
MG132
Non-CF
F508del/ F508del

turnover at the cell surface. We found that low SLC26A9 expression in F508del-expressing cells was due, at least in part, to enhanced degradation of immature SLC26A9 by the proteasome, reminiscent of F508del–CFTR. By contrast, the degradation of mature SLC26A9 appears independent of CFTR (compare *red symbols* in Fig. 6, *B* and *C*). To determine whether their very different metabolic stabilities might reflect distinct rates of endocytosis, we quantified the internalization of both proteins using a modified cell-surface biotinylation assay (see under "Experimental procedures"). There was a striking difference between their rates of endocytosis (Fig. 7). About one-fifth of the cell surface SLC26A9 was internalized within 2.5 min in cells expressing WT–CFTR or F508del–CFTR (Fig. 7, *C* and *D*), while only one-tenth of the CFTR was internalized within this time period (Fig. 7*E*). After 10 min, 44% of the cell surface SLC26A9 was endocytosed *versus* only 9.5% of WT–CFTR (Fig. 7, *A, C,* and *E*), and similar SLC26A9 internalization (50.5%) was observed in BHK cells expressing F508del–CFTR (Fig. 7, *B* and *D*). Thus, SLC26A9 endocytosis is more rapid and is independent of CFTR, and this may account for the lower metabolic stability of mature SLC26A9.

### *SLC26A9 is expressed in both ciliated and goblet cells and localizes to the tight junctions*

To localize SLC26A9, well-differentiated pHBE cell cultures were immunostained using antibodies against SLC26A9 and markers of cilia (acetylated-$\alpha$-tubulin) (30), goblet cells (mucin 5AC; MUC5AC), and undifferentiated cells (cytokeratin 14; Fig. 8). Confocal microscopy revealed SLC26A9 at the apical membrane in ciliated and goblet cells near their points of contact with neighboring cells (Fig. 8, *A–C*). Further studies confirmed expression in both these cell types but not in undifferentiated cells (Fig. 8*D*). Endogenous SLC26A9 immunostaining was co-localized with the tight junction protein zonula occludens-1 (ZO-1) (Fig. 9, *A* and *B*). We also observed some intracellular staining of SLC26A9; however, most was localized at the apical edge of the tight junction near ZO-1. Very similar results were obtained when these cells were reverse-transfected with 3HA–SLC26A9 and immunostained with anti-HA antibody (Fig. S1). To further establish the peri-junctional localization of SLC26A9, we exposed cells to EGTA for 15 min to disrupt the tight junction complexes. This caused both ZO-1 and SLC26A9 immunofluorescence to become more diffuse (Fig. 9, *C–E*). ZO-1 is a classical PDZ domain protein (PDZ; PSD-95/SAP90, Discs-large, ZO-1), and SLC26A9 has a C-terminal PDZ-binding motif; therefore, we tested whether this motif might target SLC26A9 to the tight junctions. We mutated SLC26A9 so that it lacks four amino acids at the C terminus (SLC26A9ΔPDZ). Immunofluorescence of this mutant was still near the margins of CFBE41o− cells but was displaced by ~1 $\mu$m from ZO-1 (Fig. 10*B*) compared with full-length SLC26A9 (Fig. 10, *A* and *E*). Nevertheless, the width of SLC26A9 immunofluorescence was not altered significantly (Fig. 10*F*), suggesting that the PDZ motif contributes to SLC26A9 localization near the tight junction but is not essential for its narrow distribution. By contrast, deletion of the STAS domain (*i.e.* SLC26A9ΔSTAS) did not increase the distance from ZO-1 but did cause a more diffuse spatial distribution, as indicated by the width of SLC26A9ΔSTAS immunostaining. When both deletions were combined in one mutant (SLC26A9ΔSTASΔPDZ), we observed both abnormalities, *i.e.* a loss in localization to the tight junction and a more diffuse distribution. Together, these data suggest that the PDZ-binding motif helps localize SLC26A9 near the tight junction complex, whereas the STAS domain influences its spatial organization there.

## Discussion

The $Cl^-$ conductance SLC26A9 has been proposed as a therapeutic target for the treatment of cystic fibrosis. However, Bertrand *et al.* (14) showed that the most common CF mutant F508del–CFTR reduces SLC26A9 expression and function, which would limit its utility as a drug target for most patients. In this study, we confirmed the inhibitory effect of F508del–CFTR on SLC26A9 and examined the mechanism of inhibition.

SLC26A9 cell-surface expression was higher in BHK cells when it was expressed alone or with WT–CFTR compared with when it was co-expressed with F508del–CFTR, consistent with previous results using HEK293 cells (31). This negative effect of F508del–CFTR on SLC26A9 was most pronounced in well-differentiated epithelial cells that endogenously expressed both proteins at physiological levels.

In previous studies the suppression of SLC26A9 by F580del-CFTR was found to be due, at least in part, to an increased interaction of SLC26A9 with CFTR-associated ligand (CAL) through its PDZ motif. That mechanism may account for the lysosomal (*i.e.* chloroquine-sensitive) component of SLC26A9 degradation that we have observed (Fig. 2). However, in addition to lysosomal degradation at the Golgi, many plasma membrane proteins are degraded by the endosome–lysosome pathway (32), and we observed relatively rapid SLC26A9 endocytosis that could explain the increase in SLC26A9 expression upon treatment with chloroquine (Fig. 7). Regardless, in this study we have identified an additional component of degradation that is mediated by the proteasome. Proteasomal deg-

**Figure 3. Inhibiting the proteasome increases SLC26A9 levels more in cells that express F508del–CFTR than in WT–CFTR cells.** BHK WT–CFTR (*A*) or BHK F508del–CFTR (*B*) cells were transfected with 3HA–SLC26A9 32 h before adding MG132 or CQ for 16 h. Cells were stained with mouse anti-CFTR antibody or rabbit anti-HA antibody followed by goat anti-mouse Alexa-488 or goat anti-rabbit Alexa-596 and visualized by confocal microscopy. Images are representative of $n = 20–40$ cells in three independent experiments. *C,* SLC26A9 and CFTR fluorescence intensity analyzed using ImageJ (two-way ANOVA, Bonferroni post-tests; *left:* ***, $p < 0.001$ (WT–CFTR DMSO *versus* MG-132, $p = 1.0 \times 10^{-24}$; F508del–CFTR DMSO *versus* MG-132, $p = 7.6 \times 10^{-20}$; F508del–CFTR DMSO *versus* CQ, $p = 0.0000184$, *, $p = 0.02$, interaction factor = 7.6; row factor = 129.2; column factor = 4.0; and *right:* ***, $p < 0.001$ ($p = 1.9 \times 10^{-10}$), interaction factor = 4.5; row factor = 21.3; column factor = 6.8). *D,* BHK cells stably expressing WT–CFTR (*left*) or F508del–CFTR were transiently transfected with SLC26A9 and treated with MG132 and CQ for 16 h, lysed, and subjected to SDS-PAGE and immunoblotting for SLC26A9. Blot is representative of $n = 3$ experiments. *E,* well-differentiated pHBE cells from non-CF or CF (F508del/F508del) donors treated with MG132 for 16 h, scraped, cytospun, and fixed on coverslips. SLC26A9 was stained using rabbit anti-SLC26A9 antibody, and images were taken at the apical membrane. *F,* fluorescence intensity of SLC26A9 was calculated from 39 to 57 cells in at least three independent experiments. SLC26A9 fluorescence intensity was assessed using ImageJ. Two-way ANOVA, Bonferroni post test, ***, $p < 0.001$ (non-CF *versus* F508del/F508del, $p = 1.6 \times 10^{-30}$; F508del/F508del DMSO *versus* MG132, $p = 9.3 \times 10^{-12}$), interaction factor $F = 16.8$; row factor (± MG132) $F = 200.8$; column factor (non-CF *versus* F508del/F508del) $F = 2.0$. *Scale bars*, 10 $\mu$m.

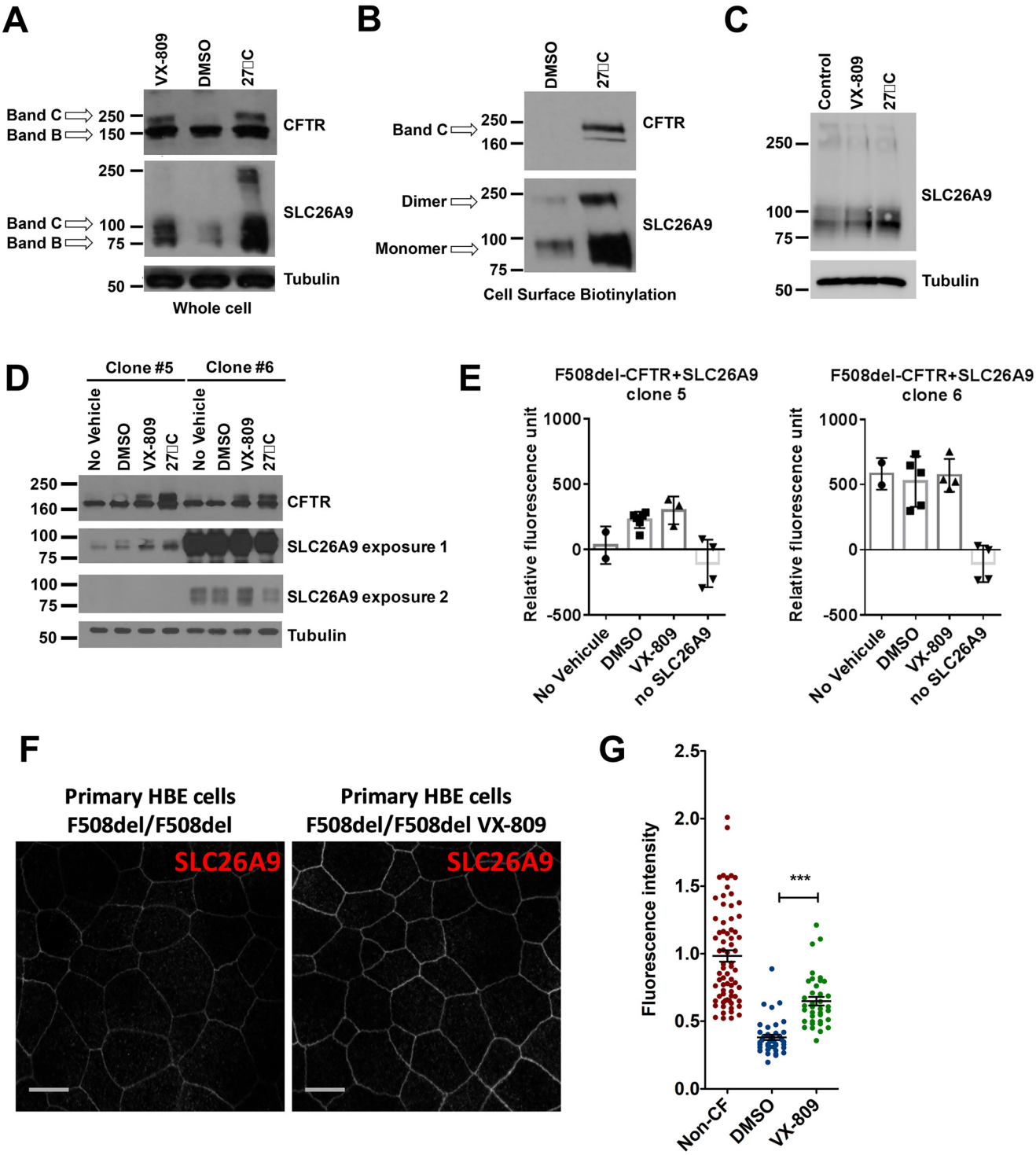


**Figure 4. Increasing cell-surface expression of F508del–CFTR also enhances both whole-cell and membrane expression of SLC26A9.** BHK–F508del (*A*) or parental (*C*) cells were transfected with SLC26A9 and exposed to VX-809 (1 $\mu$M) or low temperature (27 °C) and then lysed, and proteins were resolved by SDS-PAGE and immunoblotted. Blot is representative of four experiments. *B,* BHK–F508del cells were transiently transfected with SLC26A9 and incubated at 27 °C. Cell-surface proteins were labeled using sulfo-NHS–SS-biotin (0.5 $\mu$g/ml) and pulled down from lysates on streptavidin beads. Blot is representative of three independent experiments. *D,* double stable cell lines expressing both F508del–CFTR and SLC26A9. Two clones were selected that expressed both proteins but had very different SLC26A9 levels. Both clones were treated with VX-809 or low temperature and analyzed by immunoblotting. Blot representative of $n = 3$ independent experiments. *E,* representative measurements of membrane potential using the FLIPR membrane potential (FMP) assay performed using both clones treated with VX-809. *F,* well-differentiated pHBE cells isolated from F508del/F508del patients were treated with VX-809 (1 $\mu$M) and stained using rabbit anti-SLC26A9 antibody observed using confocal microscopy. SLC26A9 immunofluorescence was calculated in 22–48 cells from at least three independent experiments. *G,* summary of SLC26A9 immunofluorescence quantified using ImageJ. One-way ANOVA, Tukey's multiple comparison test, ***, $p = 2.3 \times 10^{-10}$, $F = 65.4$. *Scale bars,* 10 $\mu$m.

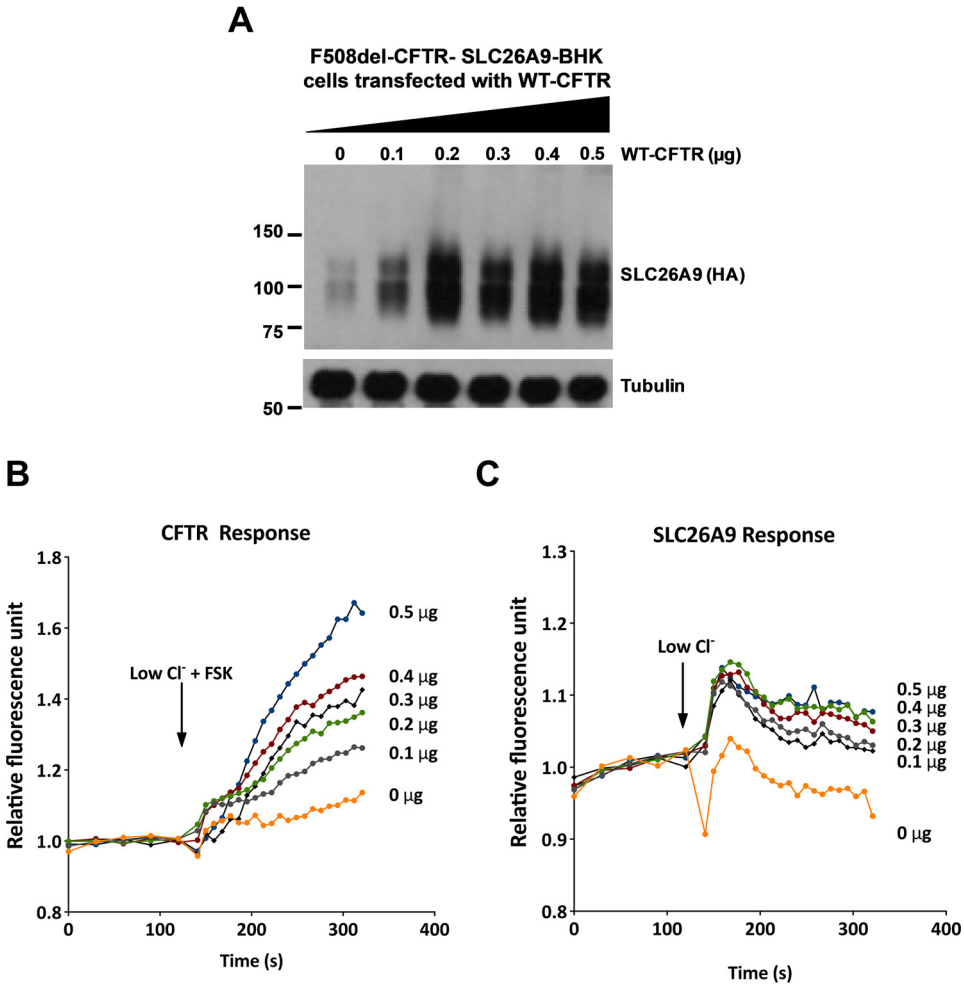


**Figure 5. SLC26A9 degradation in F508del–CFTR cells is rescued when WT–CFTR is co-expressed.** BHK–F508del cells were transfected with SLC26A9 and increasing amounts of WT CFTR plasmid (0–0.5 $\mu$g, as indicated) for 48 h. *A*, cells were lysed and proteins resolved by SDS-PAGE and immunoblotted. Blot is representative of three experiments. *B* and *C*, representative measurements of membrane potential using the FMP assay (see "Experimental procedures"). Cells were preincubated with dye in normal $Cl^-$ buffer, and then exposed to low $Cl^-$ buffer + FSK (*B*) or low $Cl^-$ buffer without FSK (*C*), and the change in fluorescence was measured.

radation became apparent during treatment with MG132, lactacystin, or bortezomid (data not shown), which caused a dramatic increase in SLC26A9 band intensity in BHK cells (Fig. 3) that was most evident in pHBE cells homozygous for F508del–CFTR. A specific retention mechanism mediated by F508del–CFTR was suggested by enhanced SLC26A9 expression after partial correction of F508del–CFTR following exposure to VX-809 or low temperature. Indeed, it was possible to titrate the inhibition by F508del–CFTR by expressing increasing amounts of WT–CFTR (Fig. 5). These data indicate that rescue of F508del–CFTR reduces SLC26A9 degradation by the proteasome.

One implication of these results is that pharmacological disruption of the SLC26A9-F508del–CFTR interaction may enhance the trafficking of mature SLC26A9 to the cell surface and increase $Cl^-$ conductance in CF cells. Clinical experience suggests that a potentiator of SLC26A9 conductance may also be required to alleviate symptoms however, because patients homozygous for G551D–CFTR still have severe CF despite relatively normal SLC26A9 trafficking (Fig. 1, *A* and *B*). WT–CFTR and F508del–CFTR have distinct interactomes (33), and the mutant probably affects many proteins besides SLC26A9. For example, in the epididymis where most CFTR localizes to tight junctions, ZO-1 levels are reduced in both CFTR knockout and F508del–CFTR mice, leading to nuclear localization of ZONAB (ZO-1 nucleic acid–binding protein), a transcription factor that controls cell growth and differentiation (34). The present results suggest that reduced expression of ZO-1 in F508del/F508del cells could also cause mislocalization or reduced expression of SLC26A9. It is interesting that PDZ interactions help co-localize CFTR and SLC26A9 with ZO-1 and that pharmacological inhibition of CFTR reduces ZO-1 expression. Together, these results suggest some role of $Cl^-$ conductance in stabilizing ZO-1, and we showed previously that the barrier function of airway epithelia depends on CFTR trafficking to cell surface (35). Sodium–hydrogen exchanger regulator factor 1 (NHERF1) expression and its distribution at the plasma membrane also depend on WT–CFTR, and NHERF1 expression is reduced in CFBE41o− cells that express F508del–CFTR (36). Whether F508del–CFTR downregulates NHERF1 and other proteins through a mechanism like the one described here for SLC26A9 remains to be deter-

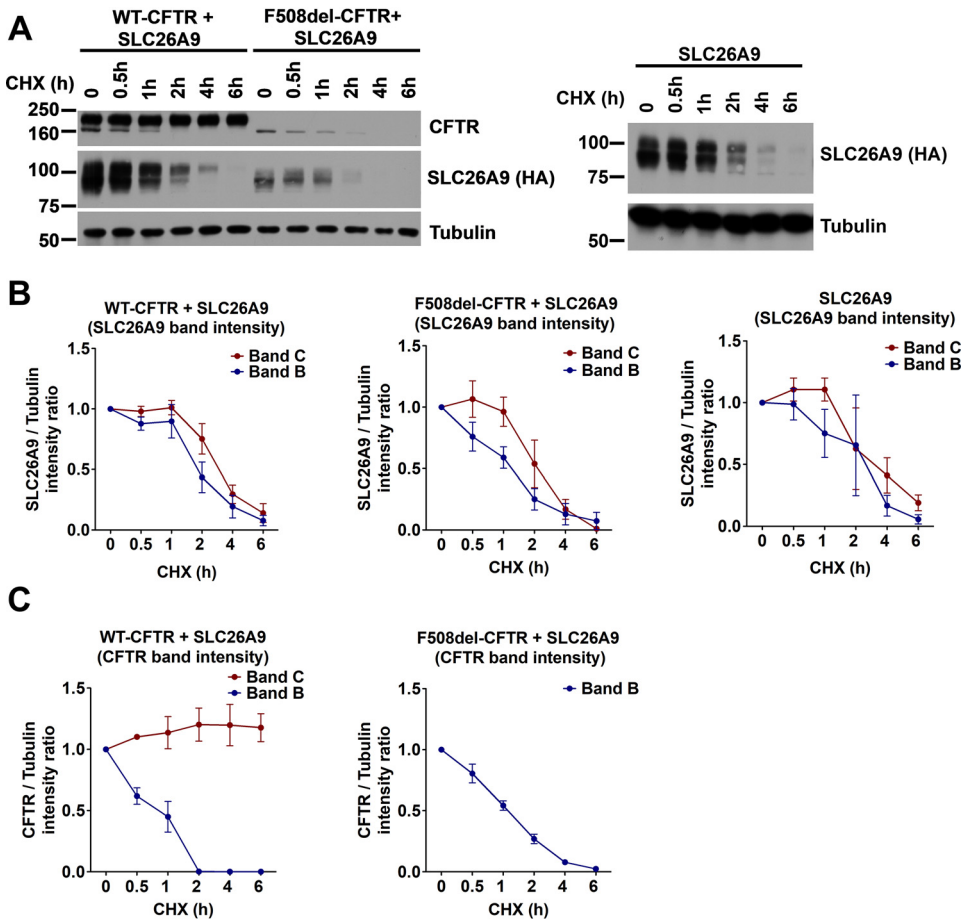


**Figure 6. Rate of SLC26A9 degradation is independent of WT–CFTR.** *A,* BHK–WT, BHK–F508del, and BHK–parental cells were transfected with SLC26A9 for 42 h prior to treatment with cycloheximide (10 $\mu$g/ml) to inhibit protein translation. Cells were lysed at indicated time points; protein was resolved by SDS-PAGE, and expression was determined by immunoblotting. Figure shows a representative immunoblot of $n = 3$ experiments. Protein expression was quantified by densitometry using ImageJ. Levels of SLC26A9 (*B*) or CFTR (*C*) normalized to tubulin at each time point. Mean ± S.E., $n = 3$.

mined. Interestingly, SLC26A4 (pendrin), another transporter hypothesized to interact with CFTR, is elevated in CF primary cells homozygous for F508del–CFTR compared with non-CF cells, probably a transcriptional up-regulation induced by pro-inflammatory signaling (37). Such differences highlight the complexity of F508del–CFTR interactions with SLC26A proteins. Interestingly, it was shown recently that the epithelial sodium channel is also localized at tight junctions very similar to what we have observed with SLC26A9, suggesting that tight junctions may be an important site of salt transport (38).

In addition to studying the effects of F508del–CFTR on SLC26A9 biogenesis and trafficking, we examined the behavior of SLC26A9 at the plasma membrane and found that it is both endocytosed (Fig. 7) and degraded more rapidly than WT–CFTR (Fig. 6). SLC26A9 expression in cells from CF patients appeared lower than in those from non-CF donors, despite the low level of WT–CFTR normally present in this cell type. Thus, SLC26A9 expression is reduced in F508del–CFTR cells that would normally have little if any CFTR immunostaining.

In summary, these results indicate that F508del–CFTR reduces SLC26A9 expression through SLC26A9 retention in the ER and premature degradation by the proteasome. Future studies should identify the site(s) of the SLC26A9–F508del–CFTR interaction so that a high-throughput biochemical assay for disrupters of the interaction can be developed to increase SLC26A9 surface expression and anion secretion in CF airways.

## Experimental procedures

### *Cell culture*

Parental BHK cells were cultured in Dulbecco's modified Eagle's medium/nutrient mixture F-12 supplemented with 100 units/ml penicillin, 100 $\mu$g/ml streptomycin, and 10% FBS. The medium for BHK cell lines stably expressing WT–CFTR or F508del–CFTR also contained 500 $\mu$M methotrexate. The medium was changed every 2 days, and cells were maintained at 37 °C in humidified air containing 5% $CO_2$. Primary human bronchial epithelial cells (HBEs) were obtained from the Primary Airway Cell Biobank at McGill University, which isolated them from tissue received from the Biobank of Respiratory Tissue at the Centre Hospitalier de l'Université de Montréal. Informed written consent was obtained from patients undergoing lung transplantations, and all procedures were approved by the Institutional Review Board of McGill University (catalog no. A08-M70-14B). The studies abide by the Declaration of Helsinki principles. Cells were cultured and differentiated using methods similar to those described by Fulcher *et al.* (41). Briefly, they were seeded onto collagen-coated polyester mem-

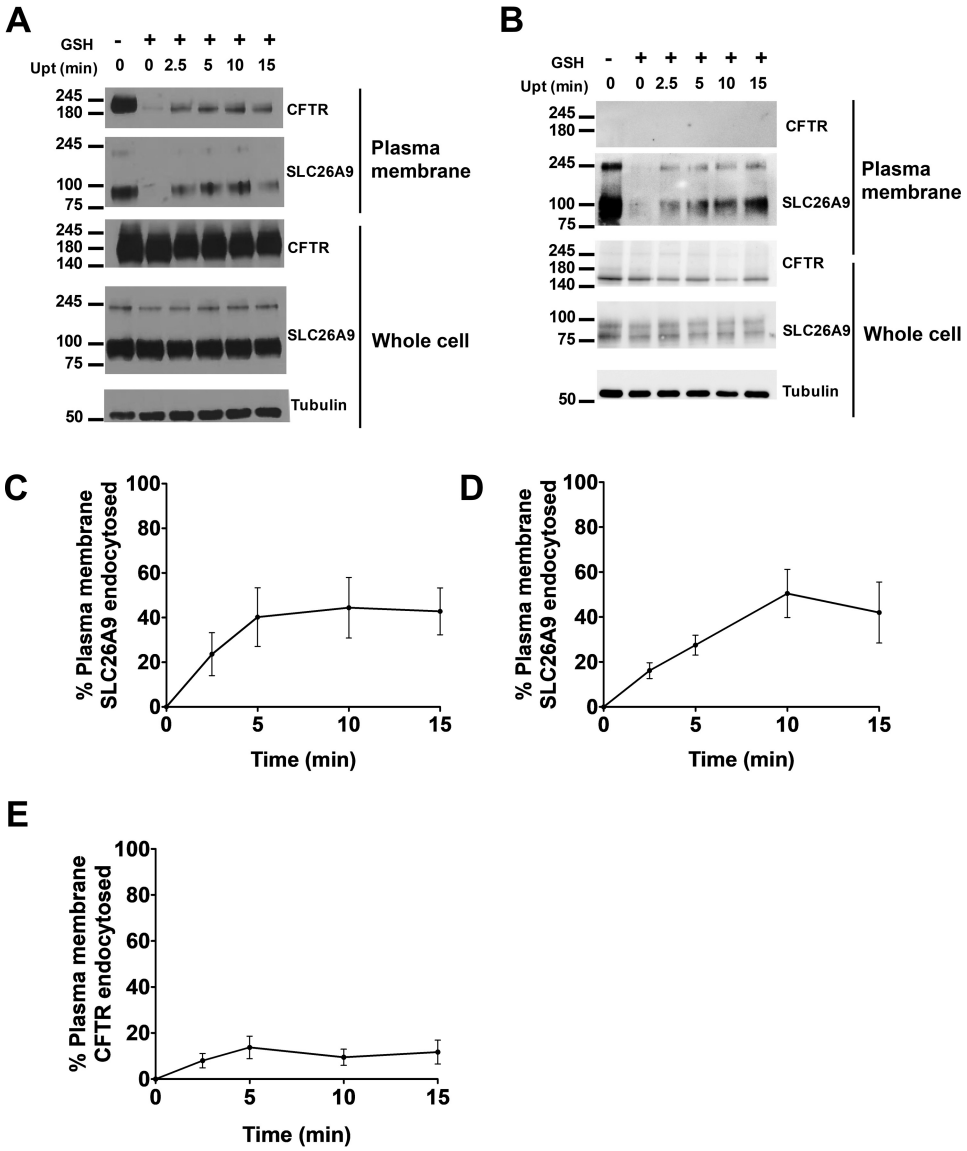


**Figure 7. SLC26A9 is endocytosed more rapidly than CFTR.** Endocytosis of SLC26A9 when co-expressed with WT–CFTR (*A*) or F508del–CFTR (*B*) was assessed by biotinylating surface proteins and incubating cells at 37 °C for 2.5, 5, 10, or 15 min. Cells were then treated with a GSH solution and lysed, and internalized biotin-labeled proteins were pulled down using streptavidin beads and detected by immunoblotting. *C,* % surface SLC26A9 endocytosed in cells co-expressing WT–CFTR. *D,* % surface SLC26A9 endocytosed in cells co-expressing F508del–CFTR. *E,* % surface CFTR endocytosed was quantified by densitometry and normalized to tubulin at each time point. Mean ± S.E., $n = 4$.

brane inserts (Corning) and remained submerged for 4 days. The apical medium was then removed, and the cells were allowed to differentiate at the air–liquid interface (ALI) for at least 21 days before use.

### *SLC26A9 construct and transfection*

SLC26A9 cDNA (NM_052934.3) was excised from PCMVSport6 and subcloned into 3HA–PCMVsport6 to generate 3HA–SLC26A9 –PCMVsport6. 3HA–SLC26A9 was then subcloned into pcDNA3.1 or pNUT. To obtain the SLC26A9 mutants (SLC26A9ΔPDZ and SLC26A9ΔSTASΔPDZ), TGA was inserted using mutagenesis at the desired site of the 3HA–SLC26A9 –pcDNA3.1 for the truncated SLC26A9 mutants. SLC26A9ΔSTAS was obtained by inserting an MluI site before and after the STAS domain and using MluI to excise the STAS domain. Constructs were transiently transfected into BHK cells using GeneJuice (Millipore) according to the manufacturer's instructions. In well-differentiated CFBE cells, polyJet (frogobio) was used to transfect the cells. Briefly, the cDNA and polyJet were added together following the manufacturer's instructions and added onto the filters. CFBE cells were then washed with PBS, trypsinized, and seeded onto the filter containing the polyJet transfection solution. The following day, cells were put in ALI conditions and cultured for 1 week.

### *Immunofluorescence imaging*

BHK cells were cultured on glass coverslips and transfected using GeneJuice and fixed 48 h later in 4% paraformaldehyde (PFA) for 15 min at room temperature. Samples were then permeabilized using 0.5% Triton X-100, blocked with 1% BSA, and immunostained using either anti-HA (Sigma, 1:200), anti-CFTR (596, mAb CFFT, 1:200), or anti-SLC26A9 (Novus Bio-

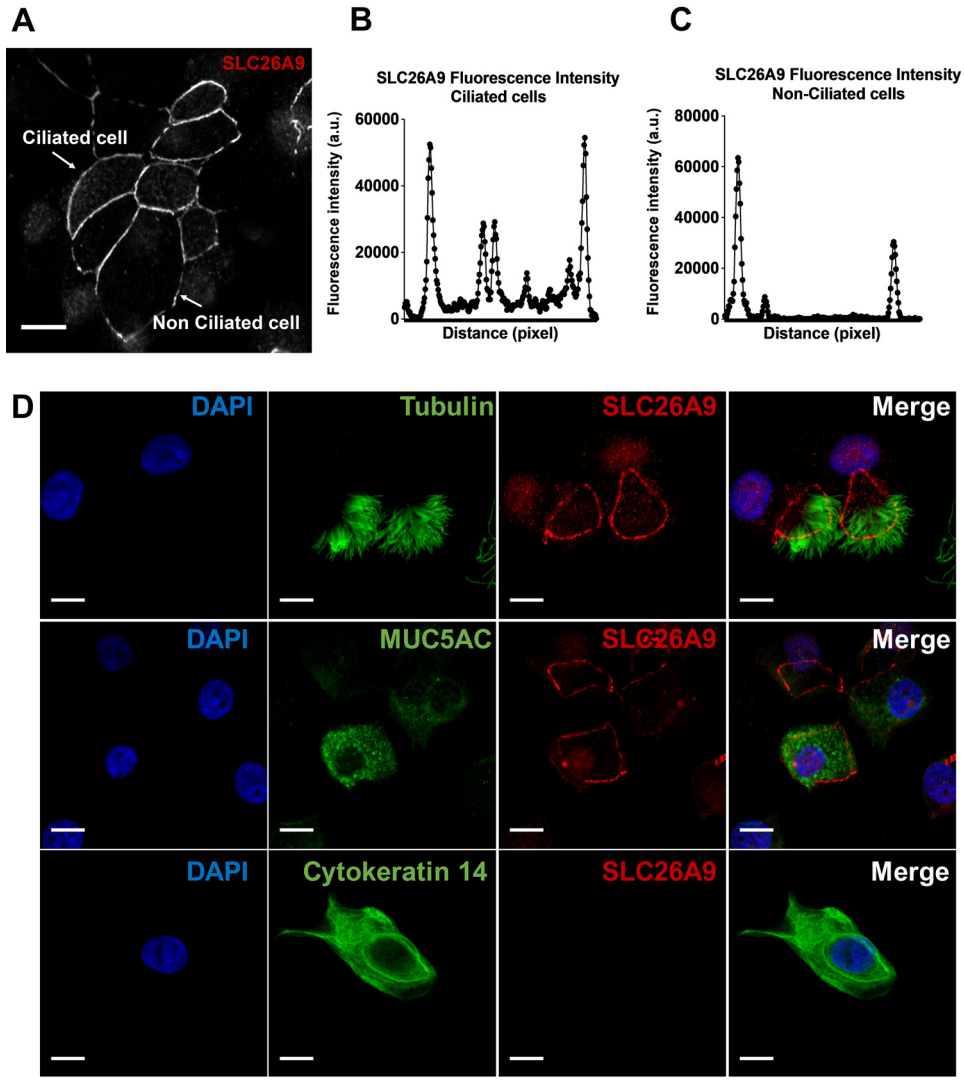


**Figure 8. SLC26A9 is expressed in ciliated and goblet cells.** Well-differentiated primary human bronchial epithelial cells from a non-CF donor were scraped, cytospun, fixed and then immunostained and imaged by confocal microscopy. Images are representative of $n = 20$ cells in three experiments. *A,* representative image of SLC26A9 immunostaining in non-CF pHBE cells. *B,* fluorescence intensity plot across a ciliated cell showing fluorescence predominantly at the cell margins. *C,* fluorescence intensity plot of a nonciliated cell showing a similar distribution. *D,* representative immunolocalization of SLC26A9 (*red*) for comparison with tubulin (marker for ciliated cell), MUC5AC (marker for goblet cell), and cytokeratin 14 (*green*; marker for basal cell). DAPI (4′,6-diamidino-2-phenylindole) was added to stain the nuclei. Figure is representative of 20 images in three experiments. *Scale bars*, 10 $\mu$m.

logical, 1:50) antibody for 16 h at 4 °C, followed by goat anti-mouse Alexa-488 (Thermo Fisher Scientific, 1:1000) or goat anti-rabbit Alexa-596 (Thermo Fisher Scientific 1:1000) antibody. Nuclei were stained using DAPI (Sigma, 0.5 $\mu$g/ml). Cells were mounted on an LSM 780 microscope (Zeiss) and observed at ×20 magnification. Images were collected and analyzed using Zen software.

To image well-differentiated pHBE cells, they were cultured at the air–liquid interface for 1 month, washed two times with PBS, and either fixed immediately or gently scraped and centrifuged onto coverslips at 450 rpm for 5 min using a Cytospin4, then fixed with 4% PFA, permeabilized with 0.5% Triton X-100, and blocked with 2% BSA. Cells were immunostained using anti-SLC26A9 (Novus Biological, 1:50), anti-CFTR (596, provided by T. Jensen and J. Riordan, University of North Carolina, Chapel Hill, through the CFF CFTR Antibody Distribution Program), or antibodies against tubulin, ZO1, MUC5AB, or cytokeratin 14 from Santa Cruz Biotechnology (1:200).

The intensity of SLC26A9 immunofluorescence staining was analyzed using ImageJ (40). The background was corrected, and the brightness and contrast were adjusted to visualize the feature and then kept constant between different conditions. For BHK cells, fluorescence intensity was measured in cells chosen using the "freehand selection tool." In the case of primary cells where SLC26A9 was localized to tight junctions, fluorescence intensity was measured along a line drawn across the cells, and 5–10 measurements were taken per cell and averaged to estimate the fluorescence of one cell. Images were normalized to the control condition for BHK cells or to non-CF cultures in the case of primary cells.

### *RNA extraction and quantitative real-time PCR*

Cells were seeded on 6-well plates (Corning) at a density of $10^5$ cells per well and studied at 48 h post-transfection. Alternatively, RNA was prepared from well-differentiated pHBE that had been cultured at the ALI for 1 month. RNA was extracted

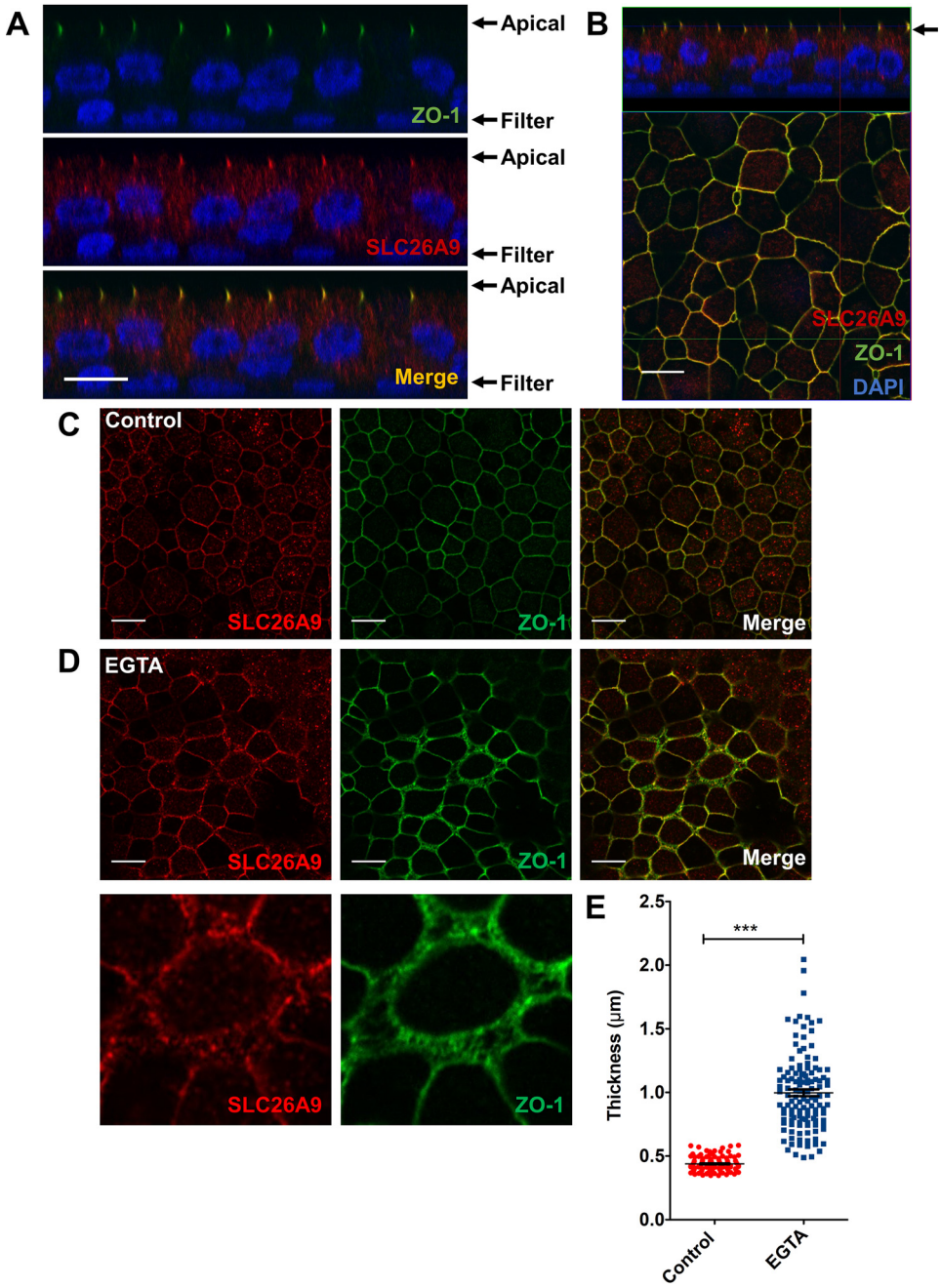


**Figure 9. SLC26A9 localizes to the tight junctions.** *A,* well-differentiated pHBE cells from non-CF patients were stained using rabbit SLC26A9 antibody, mouse ZO-1 antibody, and DAPI. Images were acquired every 0.305 $\mu$m in the *z* axis. Image is representative of $n = 10$ images from at least three different experiments. Representative image of the Z projection. *B,* representative image of apical surface. *C,* SLC26A9 (*red*) and ZO-1 (*green*) are co-localized in non-CF cells. *D,* SLC26A9 (*red*) and ZO-1 (*green*) in non-CF cells treated with EGTA for 15 min. *E,* both SLC26A9 and ZO-1 become more diffuse after disruption of the tight junctions. Figure is representative of 20–40 cells in three experiments. Student's *t* test, ***, $p < 0.001$ ($p = 1.4 \times 10^{-45}$). *Scale bars,* 10 $\mu$m.

and purified using the RNase Easy mini kit (Qiagen) following the manufacturer's instructions. For reverse transcription, 500 ng of RNA was added to 4 $\mu$l of SuperScript VILO Mastermix (Thermo Fisher Scientific) in a total volume of 20 $\mu$l for 1 h at 42 °C, and for 5 min at 85 °C. Then, 250 ng of cDNA, 10 $\mu$l of TaqMan® Fast Advanced Mastermix, and 1 $\mu$l of TaqMan® Gene Expression Assay primers in a total volume of 20 $\mu$l were added to the wells of a MicroAmp EnduraPlate™ Optical 96-Well Fast Reaction Plate. qPCR was carried out using a QuantStudio™7 Flex Real-Time PCR system with the following protocol: 20 s at 95 °C and 40 cycles at 95 °C (1 s) and 60 °C (20 s). This was followed by $\Delta\Delta Ct$ analysis.

### *Immunoblotting*

BHK cells were seeded at $1 \times 10^5$/well in 6-well plates (Corning) and studied 48 h post-transfection. They were washed three times with ice-cold PBS and then lysed in RIPA buffer containing 0.15 M NaCl, 20 mM Tris-HCl, pH 8.0, 0.08% sodium deoxycholate, 1% Triton X-100, 0.1% SDS, and protease inhibitor mixture (Roche Applied Science). 10 $\mu$g of protein was

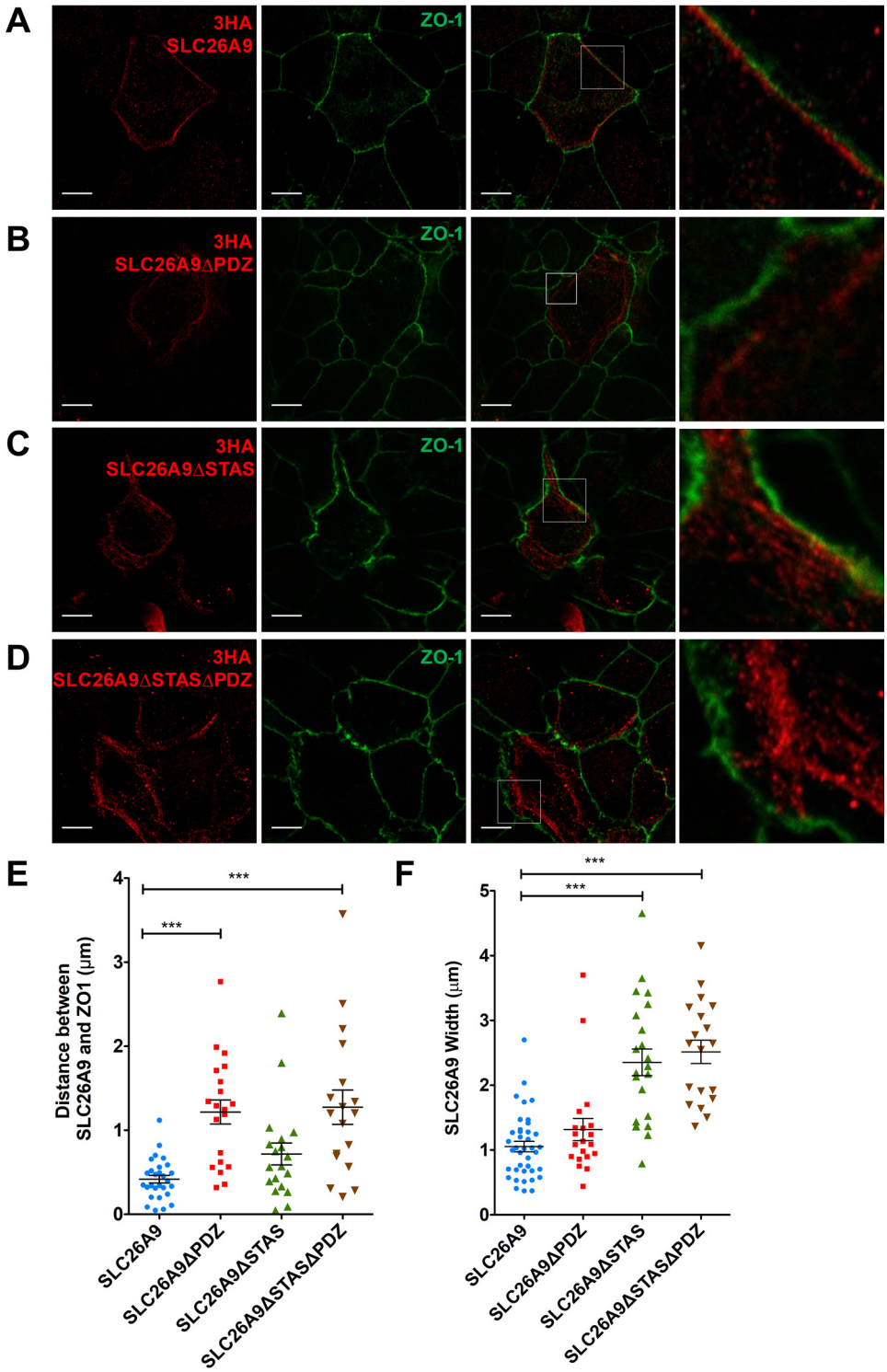


**Figure 10. Deletion of the PDZ motif but not the STAS domain causes displacement of SLC26A9 from ZO-1.** CFBE-WT–CFTR cells were reverse-transfected with 3HA–SLC26A9 or 3HA–SLC26A9 mutants and grown at air–liquid interface for 1 week prior to study. Representative confocal images of 3HA–SLC26A9 (*A*), 3HA–SLC26A9 Δ PDZ (*B*), 3HA–SLC26A9 Δ STAS (*C*), or 3HA–SLC26A9 Δ STAS Δ PDZ (*D*). Cells were stained with anti-HA (*red*) and anti-ZO-1 (*green*) antibodies. Figure is representative of 18–28 cells in at least three experiments. *E,* distance between ZO-1 and WT or mutant SLC26A9. Mean ± S.E. One-way ANOVA, Tukey's multiple comparison test (SLC26A9 *versus* SLC26A9ΔPDZ, ***, $p = 2.4 \times 10^{-7}$; SLC26A9 *versus* SLC26A9ΔSTASΔPDZ, ***, $p = 1.1 \times 10^{-5}$), $F = 11.1$. *F,* width of immunostained WT or mutant SLC26A9. Mean ± S.E. One-way ANOVA, Tukey's multiple comparison test (SLC26A9 *versus* SLC26A9ΔSTAS, ***, $p = 3.3 \times 10^{-9}$; SLC26A9 *versus* SLC26A9ΔSTASΔPDZ, ***, $p = 9.3 \times 10^{-12}$), $F = 12.5$. *Scale bars*, 10 μm.

resolved using 8% SDS-PAGE and transferred to nitrocellulose membrane. The membrane was blocked using 5% (w/v) skim milk powder in TBST (20 mM Tris-HCl, pH 7.4, 150 mM NaCl, 1% Tween 20) for 1 h at room temperature and then incubated with anti-HA (Cedarlane, 1:1000), anti-CFTR (23C5, mAb developed by our group, 1:200), or anti-tubulin (Sigma, 1:1000) for 16 h at 4 °C. The membrane was then washed four times with TBST for 15 min at room temperature, incubated with

secondary antibody for 1 h at room temperature, and washed four times with TBST. The bands were visualized using Amersham Biosciences ECL start Western blotting detecting reagent (GE Healthcare) and ChemiDoc Imaging system (Bio-Rad).

### *Cell-surface biotinylation*

Transfected BHK cells were cultured in 100-mm dishes for 48 h and washed two times with ice-cold PBS. Sulfo-NHS-SS-biotin was applied onto the cell surface for 10 min at 4 °C, and the reaction was stopped using PBS++ (PBS containing 1 mM $MgCl_2$ and 0.1 mM $CaCl_2$, pH 8.0). After washing cells with PBS++, they were lysed in RIPA buffer, and an equal amount of total protein was incubated with streptavidin-agarose beads for 2 h at 4 °C and then eluted using 2× Laemmli buffer and analyzed by immunoblotting.

### *Co-immunoprecipitation*

Transfected BHK cells were washed two times with ice-cold PBS and lysed (150 mM NaCl, 1 mM EDTA, 50 mM HEPES, 0.1% Triton X-100). The soluble lysate was precleared with Sepharose G beads for 30 min. The precleared lysates were incubated with M3A7 CFTR antibody for 30 min at 4 °C. Immunocomplexes were precipitated using Sepharose G beads. The beads were washed with lysis buffer and eluted using 2× Laemmli buffer, and analyzed by immunoblotting.

### *Endocytosis assay*

Transfected BHK cells were cultured in 60-mm dishes for 48 h and washed two times with ice-cold PBS. Sulfo-NHS-SS-biotin was applied onto the cell surface as described above and then the cells were washed and returned to the 37 °C incubator for the time period indicated. All remaining surface-biotinylated protein then was stripped at different time points using GSH buffer (50 mM GSH, 75 mM NaCl, 1 mM $MgCl_2$, 0.1 mM $CaCl_2$, 80 mM NaOH, 10% FBS, pH 8.6). Cells were subsequently lysed in RIPA buffer, and equal amounts of total protein were incubated with streptavidin-agarose beads for 2 h at 4 °C, eluted using 2× Laemmli buffer, and analyzed by immunoblotting (39).

### *FMP assay*

The FMP assay (Molecular Devices) was used to monitor changes in membrane potential. BHK cells ($10^6$) were seeded in 100-mm dishes and transfected. After 24 h, they were detached using Detachin (Genlantis, San Diego) and seeded on black 96-well, half-area, flat-bottomed microplates (Corning) 24 h prior to study. 20× stock FMP dye was diluted in normal $Cl^-$ buffer (in mM: 4.5 KCl, 115 NaCl, 1.2 $MgCl_2$, 1.2 $CaCl_2$, 10 glucose, and 10 HEPES) and exposed to cells for 30 min. Plates were then placed in the Synergy plate reader, and basal fluorescence was measured using a 530-nm laser for excitation and collecting emission at 565 nm. FMP dye (1×) in low-$Cl^-$ buffer (mM: 4.5 KCl, 115 sodium gluconate, 1.2 $MgCl_2$, 4 mM $CaCl_2$, 10 glucose, and 10 HEPES) was injected onto the cells to generate an outward $Cl^-$ gradient, and the total fluorescence of each well was measured at 8-s intervals.

### *Statistics*

Data are shown as means ± S.E. and were analyzed using Prism 5 for Mac (GraphPad software). To determine whether differences were significant, Student's *t* test and one- or two-way ANOVA with Tukey's multiple comparison post-tests were carried out as indicated in the figure legends.

*Author contributions*—Y. S., D. Y. T., and J. W. H. conceptualization; Y. S., D. Y. T., and J. W. H. resources; Y. S., J. W. H., and D. Y. T. formal analysis; D. Y. T., and J. W. H. supervision; J. W. H. and D. Y. T. funding acquisition; Y. S. validation; Y. S. investigation; Y. S. visualization; Y. S., J. W. H. and D. Y. T. methodology; Y. S. writing-original draft; Y. S., D. Y. T., and J. W. H. project administration; Y. S., D. Y. T., and J. W. H. writing-review and editing.

*Acknowledgments—We thank Carolina Martini, Elizabeth Matthes, and Julie Goepp of the Primary Airway Cell Biobank in our CF center for isolation and culture of pHBE cells. We also thank Renaud Robert for valuable input.*

### References

1. Widdicombe, J. H., and Widdicombe, J. G. (1995) Regulation of human airway surface liquid. *Respir. Physiol.* **99,** 3–12 CrossRef Medline
2. Frizzell, R. A., and Hanrahan, J. W. (2012) Physiology of epithelial chloride and fluid secretion. *Cold Spring Harb. Perspect. Med.* **2,** a009563 CrossRef Medline
3. Riordan, J. R., Rommens, J. M., Kerem, B., Alon, N., Rozmahel, R., Grzelczak, Z., Zielenski, J., Lok, S., Plavsic, N., and Chou, J.-L. (1989) Identification of the cystic fibrosis gene: cloning and characterization of complementary DNA. *Science* **245,** 1066–1073 CrossRef Medline
4. Boucher, R. C. (2007) Airway surface dehydration in cystic fibrosis: pathogenesis and therapy. *Annu. Rev. Med.* **58,** 157–170 CrossRef Medline
5. Welsh, M. J., and Smith, A. E. (1993) Molecular mechanisms of CFTR chloride channel dysfunction in cystic fibrosis. *Cell* **73,** 1251–1254 CrossRef Medline
6. Reisin, I. L., Prat, A. G., Abraham, E. H., Amara, J. F., Gregory, R. J., Ausiello, D. A., and Cantiello, H. F. (1994) The cystic fibrosis transmembrane conductance regulator is a dual ATP and chloride channel. *J. Biol. Chem.* **269,** 20584–20591 Medline
7. Higgins, C. F. (1995) The ABC of channel regulation. *Cell* **82,** 693–696 CrossRef Medline
8. Winter, M. C., and Welsh, M. J. (1997) Stimulation of CFTR activity by its phosphorylated R domain. *Nature* **389,** 294–296 CrossRef Medline
9. Matsui, H., Grubb, B. R., Tarran, R., Randell, S. H., Gatzy, J. T., Davis, C. W., and Boucher, R. C. (1998) Evidence for periciliary liquid layer depletion, not abnormal ion composition, in the pathogenesis of cystic fibrosis airways disease. *Cell* **95,** 1005–1015 CrossRef Medline
10. Smith, J. J., Travis, S. M., Greenberg, E. P., and Welsh, M. J. (1996) Cystic fibrosis airway epithelia fail to kill bacteria because of abnormal airway surface fluid. *Cell* **85,** 229–236 CrossRef Medline
11. Lukacs, G. L., Chang, X.-B., Bear, C., Kartner, N., Mohamed, A., Riordan, J. R., and Grinstein, S. (1993) The ΔF508 mutation decreases the stability of cystic fibrosis transmembrane conductance regulator in the plasma membrane. *J. Biol. Chem.* **269,** 21592–21598 Medline
12. Ward, C. L., Omura, S., and Kopito, R. R. (1995) Degradation of CFTR by the ubiquitin–proteasome pathway. *Cell* **83,** 121–127 CrossRef Medline
13. Sampson, H. M., Lam, H., Chen, P.-C., Zhang, D., Mottillo, C., Mirza, M., Qasim, K., Shrier, A., Shyng, S.-L., Hanrahan, J. W., and Thomas, D. Y. (2013) Compounds that correct F508del–CFTR trafficking can also correct other protein trafficking diseases: an *in vitro* study using cell lines. *Orphanet J. Rare Dis.* **8,** 11 CrossRef Medline
14. Bertrand, C. A., Zhang, R., Pilewski, J. M., and Frizzell, R. A. (2009) SLC26A9 is a constitutively active, CFTR-regulated anion conductance in

human bronchial epithelia. *J. Gen. Physiol.* **133,** 421–438 CrossRef Medline
15. Chang, M.-H., Plata, C., Zandi-Nejad, K., Sindić, A., Sussman, C. R., Mercado, A., Broumand, V., Raghuram, V., Mount, D. B., and Romero, M. F. (2009) Slc26a9—Anion exchanger, channel and Na+ transporter. *J. Membr. Biol.* **228,** 125–140 CrossRef Medline
16. Chang, M.-H., Plata, C., Sindic, A., Ranatunga, W. K., Chen, A.-P., Zandi-Nejad, K., Chan, K. W., Thompson, J., Mount, D. B., and Romero, M. F. (2009) Slc26a9 is inhibited by the R-region of the cystic fibrosis transmembrane conductance regulatorvia the STAS domain. *J. Biol. Chem.* **284,** 28306–28318 CrossRef Medline
17. Avella, M., Loriol, C., Boulukos, F., and Ehrenfeld, J. (2011) SLC26A9 stimulates CFTR expression and function in human bronchial cell lines. *J. Cell. Physiol.* **226,** 212–223 CrossRef Medline
18. Lohi, H., Kujala, M., Makela, S., Lehtonen, E., Kestila, M., Saarialho-Kere, U., Markovich, D., and Kere, J. (2002) Functional characterization of three novel tissue-specific anion exchangers SLC26A7, -A8, and -A9. *J. Biol. Chem.* **277,** 14246–14254 CrossRef Medline
19. Xu, J., Henriksnäs, J., Barone, S., Witte, D., Shull, G. E., Forte, J. G., Holm, L., and Soleimani, M. (2005) SLC26A9 is expressed in gastric surface epithelial cells, mediates $Cl^-/HCO_3^-$ exchange, and is inhibited by $NH_4$. *Am. J. Physiol. Cell Physiol.* **289,** C493–C505 CrossRef Medline
20. Anagnostopoulou, P., Riederer, B., Duerr, J., Michel, S., Binia, A., Agrawal, R., Liu, X., Kalitzki, K., Xiao, F., Chen, M., Schatterny, J., Hartmann, D., Thum, T., Kabesch, M., Soleimani, M., *et al.* (2012) SLC26A9-mediated chloride secretion prevents mucus obstruction in airway inflammation. *J. Clin. Invest.* **122,** 3629–3634 CrossRef Medline
21. Strug, L. J., Gonska, T., He, G., Keenan, K., Ip, W., Boëlle, P.-Y., Lin, F., Panjwani, N., Gong, J., Li, W., Soave, D., Xiao, B., Tullis, E., Rabin, H., Parkins, M. D., *et al.* (2016) Cystic fibrosis gene modifier SLC26A9modulates airway response to CFTR-directed therapeutics. *Hum. Mol. Genet.* **25,** 4590–4600 CrossRef Medline
22. Blackman, S. M., Commander, C. W., Watson, C., Arcara, K. M., Strug, L. J., Strug, L. J., Stonebraker, J. R., Wright, F. A., Rommens, J. M., Song, J. L., Kaneko, S., Sun, L., Pace, R. G., Norris, S. A., Durie, P. R., *et al.* (2013) Genetic modifiers of cystic fibrosis-related diabetes. *Diabetes* **62,** 3627–3635 CrossRef Medline
23. Sun, L., Rommens, J. M., Corvol, H., Li, W., Li, X., Chiang, T. A., Lin, F., Dorfman, R., Busson, P.-F., Parekh, R. V., Zelenika, D., Blackman, S. M., Corey, M., Doshi, V. K., Henderson, L., *et al.* (2012) Multiple apical plasma membrane constituents are associated with susceptibility to meconium ileus in individuals with cystic fibrosis. *Nat. Genet.* **44,** 562–569 CrossRef Medline
24. Li, W., Soave, D., Miller, M. R., Keenan, K., Lin, F., Gong, J., Chiang, T., Stephenson, A. L., Durie, P., Rommens, J., Sun, L., and Strug, L. J. (2014) Unraveling the complex genetic model for cystic fibrosis: pleiotropic effects of modifier genes on early cystic fibrosis-related morbidities. *Hum. Genet.* **133,** 151–161 CrossRef Medline
25. Li, J., Xia, F., and Reithmeier, R. A. (2014) *N*-Glycosylation and topology of the human SLC26 family of anion transport membrane proteins. *Am. J. Physiol. Cell Physiol.* **306,** C943–C960 CrossRef Medline
26. Bozoky, Z., Krzeminski, M., Muhandiram, R., Birtley, J. R., Al-Zahrani, A., Thomas, P. J., Frizzell, R. A., Ford, R. C., and Forman-Kay, J. D. (2013) Regulatory R region of the CFTR chloride channel is a dynamic integrator of phospho-dependent intra- and intermolecular interactions. *Proc. Natl. Acad. Sci. U.S.A.* **110,** E4427–E4436 CrossRef Medline
27. Cheng, J., Moyer, B. D., Milewski, M., Loffing, J., Ikeda, M., Mickle, J. E., Cutting, G. R., Li, M., Stanton, B. A., and Guggino, W. B. (2002) A Golgi-associated PDZ domain protein modulates cystic fibrosis transmembrane regulator plasma membrane expression. *J. Biol. Chem.* **277,** 3520–3529 CrossRef Medline
28. Bergbower, E., Boinot, C., Sabirzhanova, I., Guggino, W., and Cebotaru, L. (2018) The CFTR-associated ligand arrests the trafficking of the mutant ΔF508 CFTR channel in the ER contributing to cystic fibrosis. *Cell. Physiol. Biochem.* **45,** 639–655 CrossRef Medline
29. Glozman, R., Okiyoneda, T., Mulvihill, C. M., Rini, J. M., Barriere, H., and Lukacs, G. L. (2009) *N*-Glycans are direct determinants of CFTR folding and stability in secretory and endocytic membrane traffic. *J. Cell Biol.* **184,** 847–862 CrossRef Medline
30. Al-Bassam, J., and Corbett, K. D. (2012) α-Tubulin acetylation from the inside out. *Proc. Natl. Acad. Sci. U.S.A.* **109,** 19515–19516 CrossRef Medline
31. Bertrand, C. A., Mitra, S., Mishra, S. K., Wang, X., Zhao, Y., Pilewski, J. M., Madden, D. R., and Frizzell, R. A. (2017) The CFTR trafficking mutation F508del inhibits the constitutive activity of SLC26A9. *Am. J. Physiol. Lung Cell. Mol. Physiol.* **312,** L912–L925 CrossRef Medline
32. Schulze, H., Kolter, T., and Sandhoff, K. (2009) Principles of lysosomal membrane degradation: cellular topology and biochemistry of lysosomal lipid degradation. *Biochim. Biophys. Acta* **1793,** 674–683 CrossRef Medline
33. Pankow, S., Bamberger, C., Calzolari, D., Martínez-Bartolomé, S., Lavallée-Adam, M., Balch, W. E., and Yates, J. R., 3rd. (2015) ΔF508 CFTR interactome remodelling promotes rescue of cystic fibrosis. *Nature* **528,** 510–516 CrossRef Medline
34. Ruan, Y. C., Wang, Y., Da Silva, N., Kim, B., Diao, R. Y., Hill, E., Brown, D., Chan, H. C., and Breton, S. (2014) CFTR interacts with ZO-1 to regulate tight junction assembly and epithelial differentiation through the ZONAB pathway. *J. Cell Sci.* **127,** 4396–4408 CrossRef Medline
35. LeSimple, P., Liao, J., Robert, R., Gruenert, D. C., and Hanrahan, J. W. (2010) Cystic fibrosis transmembrane conductance regulator trafficking modulates the barrier function of airway epithelial cell monolayers. *J. Physiol.* **588,** 1195–1209 CrossRef Medline
36. Guerra, L., Fanelli, T., Favia, M., Riccardi, S. M., Busco, G., Cardone, R. A., Carrabino, S., Weinman, E. J., Reshkin, S. J., Conese, M., and Casavola, V. (2005) Exchanger regulatory factor isoform 1 overexpression modulates cystic fibrosis transmembrane conductance regulator (CFTR) expression and activity in human airway 16HBE14o cells and rescues F508 CFTR functional expression in cystic fibrosis cells. *J. Biol. Chem.* **280,** 40925–40933 CrossRef Medline
37. Kim, D., Huang, J., Billet, A., Abu-Arish, A., Goepp, J., Matthes, E., Tewfik, M. A., Frenkiel, S., and Hanrahan, J. W. (2019) Pendrin mediates bicarbonate secretion and enhances CFTR function in airway surface epithelia. *Am. J. Respir. Cell Mol. Biol.* **60,** 705–716 CrossRef Medline
38. Musante, I., Scudieri, P., Venturini, A., Guidone, D., Caci, E., Castellani, S., Conese, M., and Galietta, L. J. V. (2019) Peripheral localization of the epithelial sodium channel in the apical membrane of bronchial epithelial cells. *Exp. Physiol.* **104,** 866–875 CrossRef Medline
39. Bomberger, J. M., Guggino, W. B., and Stanton, B. A. (2011) Methods to monitor cell surface expression and endocytic trafficking of CFTR in polarized epithelial cells. *Methods Mol. Biol.* **741,** 271–283 CrossRef Medline
40. Rasband, W. S. (2011) *ImageJ*. National Institutes of Health, Bethesda
41. Fulcher, M. L., Gabriel, S., Burns, K. A., Yankaskas, J. R., and Randell, S. H. (2005) Well-differentiated human airway epithelial cell cultures. in *Human Cell Culture Protocols* (Picot, J. ed.) 2nd Ed., pp. 183–206, Humana Press